



Published in final edited form as:

J Immunol. 2015 June 1; 194(11): 5200–5210. doi:10.4049/jimmunol.1500221.

Collecting lymphatic vessel permeability facilitates adipose tissue inflammation and distribution of antigen to lymph node-homing adipose tissue DCs

Emma L. Kuan^{*}, Stoyan Ivanov[†], Eric A. Bridenbaugh[‡], Gabriel Victora[§], Wei Wang[‡], Ed W. Childs[¶], Andrew M. Platt^{*}, Claudia V. Jakubzick^{||}, Robert J. Mason[#], Anatoliy A. Gashev[‡], Michel Nussenzweig^{††}, Melody A. Swartz^{‡‡}, Michael L. Dustin[§], David C. Zawieja[‡], and Gwendalyn J. Randolph^{†,*}

^{*}Department of Gene and Cell Medicine, Graduate Program in Immunology and Immunology Institute, Mount Sinai School of Medicine, New York, NY 10029 USA [†]Department of Pathology & Immunology, Washington University School of Medicine, St. Louis, MO 63110 USA [‡]Department of Systems Biology and Translational Medicine, Division of Lymphatic Biology, Cardiovascular Research Institute, Texas A&M Health Science Center College of Medicine, Temple, TX 76504 USA [¶]Department of Surgery, Cardiovascular Research Institute, Texas A&M Health Science Center College of Medicine, Temple, TX 76504 USA [§]Program in Molecular Pathogenesis, Skirball Institute for Biomolecular Medicine, The Helen L. and Martin S. Kimmel Center for Biology and Medicine, New York University School of Medicine, New York NY 10016 USA ^{||}Department of Pediatrics, National Jewish Health, Denver, CO 80206 [#]Department of Medicine, National Jewish Health, Denver, CO 80206 ^{††}Laboratory of Molecular Immunology and Howard Hughes Medical Institute, The Rockefeller University, New York, NY 10065 USA ^{‡‡}Institute of Bioengineering, Ecole Polytechnique Fédérale de Lausanne (EPFL), Lausanne 1015, Switzerland

Abstract

Collecting lymphatic vessels (CLVs), surrounded by fat and endowed with contractile muscle and valves, transport lymph from tissues after it is absorbed into lymphatic capillaries. CLVs are not known to participate in immune responses. Here, we observed that the inherent permeability of CLVs allowed broad distribution of lymph components within surrounding fat for uptake by adjacent macrophages and dendritic cells (DCs) that actively interacted with CLVs. Endocytosis of lymph-derived antigens by these cells supported recall T cell responses in the fat and also generated antigen-bearing DCs for emigration into adjacent lymph nodes. Enhanced recruitment of DCs to inflammation-reactive lymph nodes significantly relied on adipose tissue DCs to maintain sufficient numbers of antigen-bearing DCs as the lymph node expanded. Thus, CLVs coordinate inflammation and immunity within adipose depots and foster the generation of an unexpected pool of APCs for antigen transport into the adjacent lymph node.

Introduction

Absorptive lymphatic capillaries with blind-ended termini are positioned in the parenchyma of most organs (1) and consist of a single layer of lymphatic endothelial cells with elegantly organized intercellular junctions (2). Lymphatic capillaries take up fluid, macromolecules, and immune cells including dendritic cells (DCs) and T cells that traverse afferent lymphatic vessels en route to lymph nodes (LNs) (1-6). In the intestine, lymphatic capillaries, called lacteals, are crucial for absorption of chylomicrons. Before reaching the LN, lymphatic capillaries converge successively into afferent collecting lymphatic vessels that no longer serve an absorptive function for either molecules or cells. Instead, collecting vessels, distinguished by luminal valves and an organized wall containing contractile cells that promote lymph propulsion(3), are specialized for efficient transport of lymph and its contents to the draining LN and ultimately beyond the node in efferent lymphatic vessels (1).

As collecting vessels leave the parenchyma of organs and extend to the LN, they are encased in white adipose tissue (1, 7). In contrast to lymphatic capillaries, cells of the immune system have not been found to enter collecting lymphatic vessels (6). Hence, collecting vessels have received little consideration as players in innate or adaptive immunity, but instead have been viewed simply as conduits for immune cell passage to and from LNs. Furthermore, the historical view has been that collecting lymphatics are relatively impermeable to solutes (8), in addition to cells, reinforcing the general idea that these vessels solely function in lymph transport. However, recently the notion of the impermeability of collecting lymphatics to macromolecules was refuted by the demonstration that muscular collecting lymphatics of the rat mesentery are as permeable to macromolecules, such as albumin (65 kDa), as the adjacent venules (4). Transport of macromolecules across the collecting lymphatic wall is coupled to water flux and sensitive to lymph pressure (4). It remains unknown whether and how the unexpected physiological permeability of lymphatic collecting vessels affects the surrounding adipose tissue. In conditions of reduced lymphatic integrity due to haplo-insufficiency of the key lymphatic transcription factor Prox-1, mesenteric lymphatics appear especially leaky and this leakiness may drive adipocyte expansion and obesity (9).

In this study, we characterized collecting lymphatic vessels in a broad range of adipose tissues from mice, rats, and human subjects with respect to their relationship with MHC II⁺ cells of the immune system. Then, in the mouse, we tracked the fate of soluble antigens from the point of tissue delivery to the draining LN and focused on the typically discarded white adipose tissue (perinodal adipose tissue, PAT) rich in collecting lymphatic vessels that is upstream of the LN. We show that the inherent permeability of collecting lymphatic vessels can lead to several related consequences, including the onset of inflammation in PAT in response to inflammatory stimulants flowing in lymph, local presentation of lymph-derived antigens to these fat depots, and arming PAT dendritic cells (DCs) with antigen. We had earlier reported that adjuvant-reactive lymph nodes remodel as part of a coordinated inflammatory program to allow increased numbers of antigen-transporting DCs to enter the inflamed lymph nodes (10). A major source for these cells appears to be the PAT DCs that have acquired lymph-derived antigens.

Materials and Methods

Animals

Seven to nine-week-old male mice were studied, including standard CD45.2⁺ (Ly5.2) WT (Jackson Laboratories) mice, CD45.1⁺ (Ly5.1) congenic mice (NCI), plt/plt mice ((11); maintained at Mount Sinai), TCR-transgenic TEa mice (12) (shared with us by J.S. Bromberg), CD11c-EYFP mice ((13); maintained at Rockefeller University), or CCR7-deficient mice (stock # 005794, Jackson Laboratories) all bred onto the C57BL/6 background. K14-VEGFR-3-Ig mice and control littermates on a mixed background were previously described (14). Mice were housed in a specific pathogen-free environment at Mount Sinai School of Medicine, Rockefeller University, or Ecole Polytechnique Fédérale de Lausanne and were used in accordance with institutional and federal policies. Male Sprague-Dawley and CrI:CD (SD) rats (150–300 g) were purchased from Harlan Laboratories or Charles River, respectively, housed at Texas A&M AAALAC accredited animal facilities, and were used in accordance with institutional and federal policies.

Human tissue

With approval of The Committee for the Protection of Human Subjects at National Jewish Health, de-identified human lungs and associated LNs not suitable for transplantation and donated for medical research were obtained from the National Disease Research Interchange (Philadelphia, PA, USA) and the International Institute for the Advancement of Medicine (Edison, NJ, USA).

Fluorescent antigen tracking

FITC painting—For contact sensitization (FITC painting assay), fluorescein isothiocyanate (FITC; Sigma-Aldrich) was dissolved in acetone and dibutylphthalate (1:1) at 8 mg/ml (15). Aliquots of this solution (25 μ l) were applied onto the shaved interscapular mouse skin that is drained by the brachial LN. Mice were euthanized 18 h later.

To track T cells after FITC painting, total CD4⁺ T cells were isolated from draining LNs 4 days after FITC skin painting using anti-CD4 magnetic beads (clone L3T4) (Miltenyi Biotec). Then 3.5×10^6 these purified CD4⁺ T cells or naïve CD4⁺ T cells were transferred to C57BL/6 recipient mice i.v. Five h later, some recipient mice received FITC solution applied to the back skin and ears, while others were injected i.d. with E α GFP. Approximately 36 h later, CD4⁺ T cells in draining LNs and PATs were analyzed by flow cytometry, and ear thickness was measured using fine digital calipers. Calipers were carefully placed on the ears so as to measure the thickness of the same area of the ear in different mice with the same individual performing all analysis in a semi-blinded manner in which mice in different experimental groups were identified, through their toe clip pattern, only after ear thickness was measured.

E α GFP—Plasmids containing E α GFP or E α Cherry constructs were kindly provided by M.K. Jenkins (University of Minnesota Medical School). E α GFP and E α Cherry protein induction and purification were carried out as described previously (16). Endotoxin was removed by ToxinEraser Endotoxin Removal Kit (GenScript) and measured by ToxinSensor

Chromogenic LAL Endotoxin Assay Kit (GenScript). The residual endotoxin in EαGFP and EαCherry was $\sim 8.5 \times 10^{-5}$ EU/ μg of EαGFP or EαCherry. For i.d. immunization, 40 μg of αGFP or EαCherry was injected into the dermis of the back skin. For direct delivery into PAT, the interscapular skin of anesthetized mice was shaved and a narrow opening was cut into the skin for access to the PAT around the brachial node. Four μl of EαGFP at 5 mg/ml were injected into the PAT and then the skin opening was sealed using Vetbond (3M). To track T cell proliferation and activation in mice treated with EαCherry, naïve CD4⁺ T cells from the spleen of TEa transgenic mice (12) were sorted by positive staining for CD4 and negative staining for CD44. These cells were labeled with carboxyfluorescein succinimidyl ester (CFSE) (Invitrogen) at 10 mM to follow their proliferation after injection in vivo. One million of CFSE-labeled TEa naïve CD4⁺ T cells were then i.v. injected to each C57BL/6 recipient. After 24 h, 20 μg or 40 μg of EαCherry was then i.d. or intraPAT delivered to one PAT around brachial LN or one side of scapular back skin, respectively. Proliferation and activation of transferred TEa CD4⁺ T cells were then evaluated in brachial LNs 2 days after EαCherry delivery.

Dextrans—To label skin lymphatic vessels, 10 μl of 1 % 500 kDa FITC-conjugated or 70 kDa TRITC-conjugated, lysine-fixable dextran (Molecular Probes) were injected into mouse skin 7-10 min before mice were euthanized.

Tissue Sections

For preparation of mouse tissue sections, brachial LNs and associated PAT were carefully dissected and fixed in 4 % paraformaldehyde, dehydrated in alcohol, embedded in glycol methacrylate (JB-4; Polysciences), sectioned (2- μm thickness), and visualized using epifluorescence microscopy. For immunostaining analysis in JB-4 sections, whole-mount staining of the LN and associated adipose depot was performed before embedding in JB-4 resin. Tissues were fixed in 0.5% paraformaldehyde overnight at 4° C, permeabilized in 1x PBS containing 0.1 % Tween 20 (Sigma-Aldrich) for a day at 4° C, and blocked using mouse Fc block (BD Pharmingen) for an additional day at 4° C. Then goat-anti-CCL21 (R&D) was added for 1 week, washed, and followed by Cy3- or Cy2-conjugated anti-goat (Jackson ImmunoResearch) for 3 days.

Multiphoton Microscopy

For multiphoton imaging of fixed tissue, the entire brachial LN and its PAT from mice treated with i.d EαGFP for different time points and i.d. TRITC-dextran for 7 min before sacrifice were collected and fixed in 4% paraformaldehyde overnight at 4° C. Samples then were washed in 1x PBS and fixed onto a Petri-dish with instant glue (Krazy) and then imaged using a RioRad Radiane 2000 multi-photon system mounted to a fixed-stage upright microscope with a Ti:sapphire laser pumped by a 10W Verdi tunable at 720-920 nm with a two-channel external detection system and fitted with a 20x / 0.95 NA water immersion objective. Image stacks were combined and analyzed using ImageJ or Volocity 5 (Perkin-Elmer) software.

For intravital imaging, mice were anaesthetized with 100 mg ketamine, 15 mg xylazine and 2.5 mg acepromazine per kg body weight. The hind legs of mice were shaved using a

double-edged razor blade. Mice were restrained on a stage warmer at 37 °C (BioTherm Micro S37; Biogenics) and an incision was made on the posterior side of one hind leg immediately below the knee joint. The leg was then held in position using a metal strap fixed to the stage warmer, with a small hole through which the lymphatic and adjacent fat pad could be visualized. Mice were imaged using an Olympus Fluoview FV 1000MPE multi-photon laser-scanning microscope connected to a Coherent Chameleon laser (tunable from 690-1040 nm) and an Olympus 25x/1.05 objective, controlled by FluoView (FV-10) software (Olympus) at the Rockefeller Bio-Imaging Facility. To image EGFP, EYFP, and Evan's blue, the excitation wavelength was set between 910-940 nm; emission light was split by two dichroic mirrors at 505 nm and 570 nm into three channels and band-pass filters optimized for detecting EGFP without bleed-through from EYFP (dichroic 505 nm, hq 460-510), EYFP (hq 495-540), and Evan's blue dye (hq 570-635) were used to detect fluorescent proteins. To create time-lapse sequences, we typically scanned 72×425×425 μm volumes of tissue at 6 μm Z-steps and 40 seconds intervals. Images were processed and analyzed using Volocity 5 (Perkin-Elmer) and Imaris 6 (Bitplane) software.

Flow Cytometry

Brachial or inguinal or popliteal LNs were excised, teased with needles and digested in collagenase D (Roche) for 30 min at 37° C. Cells were then lightly pressed through a 70-μm cell strainer and then washed, counted, and stained for flow cytometry.

For obtaining single cell suspension from PATs, mice were perfused with 10 ml 1x DPBS, and PATs were collected and minced into small pieces and then digested in RPMI-1640 (cellgro) media containing 0.56 units/ml of liberase blendzyme 3 (Roche) and 0.1 mg/ml of DNase I (Sigma-Aldrich) for 1 h. Tissue was then homogenized using a 20 G needle. Debris was filtered through a 70- μm cell strainer, and erythrocytes were lysed by 1x BD Pharm Lyse (BD). Cells then were washed, counted, and stained for flow cytometry.

For flow cytometry, combinations of the following mAbs were used in staining. Acquisition of samples was performed using a LSR II (BD Bioscience) instrument, and data were analyzed with Flowjo software (Tree Star). The mAbs to the following molecules were obtained from BD Pharmingen or eBioscience except where otherwise indicated: CD11b, Gr-1 (recognizes Ly6G and Ly6C), MerTK (polyclonal goat, R & D Systems), goat IgG (R & D Systems), CD45, B220, CD8, IA^b, CD25, CD3, Vα2, CD64, CD103, YAc, CD11c, CD44, CD4, Siglec F, Armenian hamster IgG isotype control, I-A;I-E, F4/80, rat IgG2a (Serotec), anti-FITC (Jackson ImmunoResearch Laboratories), mouse IgG1 isotype control. DAPI was used to gate our DAPI⁺ dead cells.

For immunostaining of single-cell suspensions, 100 μl of a suspension from LN or PATs were applied to Alcian blue-coated coverslips and then incubated in 37°C for 30 minutes, followed by fixation with 4% paraformaldehyde and washing with 1x PBS. Cells were permeabilized for 15 minutes at RT with medium containing 0.05 % saponin (Sigma-Aldrich), 10 % goat serum, and 10 mM glycine. Primary antibodies, including Armenian hamster-anti-CD11c (eBioscience), mouse-anti-IA^b (BD Biosciences), were used and followed by secondary antibodies, Cy3-conjugated anti-Armenian hamster, Cy5-conjugated

anti-mouse, or Cy2-conjugated anti-FITC for detection. DAPI (100 ng/ml) solution was used for nuclei staining.

Optical projection tomography

TRITC-dextran (70 KDa) was i.d. injected into WT mouse upper scapular skin for lymphatic vessel labeling. Ten min. later, Alexa Fluor 488-dextran (3 KDa) was injected intravenously for blood vessel labeling. Mice were sacrifice 5 min after and brachial LN and adipose tissue around it were collected together as a whole tissue and then was fixed in 4 % paraformaldehyde. Fixed tissue was sent to Bioptonics (Edinburgh, Scotland, United Kingdom) for further processing and scanning.

Quantitative real-time PCR

Total RNA was extracted from whole frozen PATs first homogenized with Dounce homogenizer. TRIZOL-LS (Invitrogen) was added and the RNeasy mini kit (Qiagen) was followed. First-strand cDNA was synthesized using SuperScript II Reverse Transcriptase (Invitrogen). To amplify cDNA, 2x SYBR Green JumpStart Taq ReadyMix for Quantitative PCR (Sigma) was used, and then real-time quantitative PCR was carried out in the Quantitative PCR Shared Resource Facility in Mount Sinai School of Medicine using the **ABI PRISM 7900HT** instrument. PCR cycling conditions were 95°C for 2 minutes for polymerase activation, then amplification for 40 cycles: 95°C for 15 seconds, 55°C for 15 seconds, and 72 for 30 seconds. Relative expression levels were calculated using *Gapdh* as endogenous control.

Primer sequences were as follows: *Tnfa* forward, 5'-GACCCTCACTCAGATCATCTTCT-3'; *Tnfa* reverse, 5'-CCACTTGGTGGTTTGCTACGA-3'. *Il6* forward, 5'-CGGCAAACCTAGTGCGTTAT-3'; *Il6* reverse, 5'-TCTGACCACAGTGAGGAATGTC-3'. *iNos* forward, 5'-ACTGGGGCAGTGGAGAGATT-3'; *iNos* reverse, 5'-GGTCAAACCTTTGGGGTTGA-3'. *Tlr4* forward, 5'-GCAGAAAATGCCAGGATGATG-3'; *Tlr4* reverse, 5'-AACTACCTCTATGCAGGGATTCAAG-3'. *Ccr2* forward, 5'-GGGAGACAGCAGATCGAGT-3'; *Ccr2* reverse, 5'-TCCCTCCTCCCTGCTTAAA-3'. *Mcp-1* forward, 5'-GGCTCAGCCAGATGCAGTTA-3'; *Mcp-1* reverse, 5'-CCTACTCATTGGGATCATCT-3'. *Cd36* forward, 5'-TTGTACCTATACTGTGGCTA-3'; *Cd36* reverse, 5'-CTTGTGTTTTGAACATTCT-3'.

Rat Mesenteric Lymphatic Immunostaining and Imaging

For isolated vessel immunostaining, fixed lymphatics were incubated in blocking solution (1% bovine serum albumin (BSA), 5% normal goat serum in PBS) for 1 hr at room temperature (RT) and then divided into 2 pieces. The two sections were incubated in blocking solution overnight at 4°C in the presence of intra- and extralumenal primary antibodies or the corresponding normal immunoglobulins (negative-control), respectively. The vessel sections were washed intra- and extralumenally in PBS 3 times for 5 min each and then intra- and extralumenally incubated with secondary antibodies for 1 h at RT. The vessel sections were again intra- and extralumenally washed with PBS 3 times for 5 min

each and then cannulated and tied onto 2 glass pipettes, pressurized to 2 cm H₂O, and secured to the stage of the confocal microscope for immediate observation.

For whole-mount immunostaining, the intestines and associated mesenteries were exteriorized and dissected distal to the duodenojejunal flexure, proximal to the cecum, and dorsal to the mesenteric LNs, respectively, and placed in Dulbecco's PBS (DPBS) with 10 g/L bovine serum albumin at RT. The intestine/mesentery was pinned into a silicone-coated petri dish, rinsed 3 times with DPBS, incubated in acetone for 20 min at 4°C, and washed in PBS 4 times for 10 min each. Mesenteric panels (~20 by 50 mm) containing blood and lymphatic vessels were isolated and incubated 1 hr at RT in blocking solution. The samples were then incubated 18 h at 4°C in blocking solution containing primary antibodies. Negative controls were prepared as above. The samples were washed 3 times for 20 min each in PBS before incubation for 2 h at RT in PBS containing 1% BSA and secondary antibodies. The samples were washed 3 times for 20 min each followed by 30 min in PBS before being spread onto glass slides, dried, and mounted under coverslips with ProLong Gold Antifade Reagent (Invitrogen).

Primary antibodies used include mouse-anti-eNOS (IgG1, clone3, BD Transduction Lab.), mouse anti-rat PECAM-1 (IgG1, clone TLD-3A12, BD Transduction Lab.), mouse-anti-MHC II (IgG2a, clone 10.3.6, Santa Cruz BioTechnology), and rabbit anti- α smooth muscle actin (ab5694, Abcam, Cambridge, MA). Secondary antibodies include goat anti-mouse-IgG1-Alexa Fluor 488, goat anti-mouse IgG2a-Alexa Fluor 647, and donkey-anti-rabbit-Alexa Fluor 594 (Invitrogen). All antibody concentrations were approximately 10 μ g/ml.

The samples were imaged using a Leica TCS SP2 AOBS confocal microscope (Leica Microsystems) with either a Leica HC PL APO 20X (dry, 0.7 na) or a Leica U APO 340/cc 40X (water immersion, 1.15 na) objective. 0.5 μ m z-axis steps were taken with a 1 airy disk pinhole at multiple sites within each sample. The samples were excited with an argon ion laser at 488 nm and a He-Ne laser at 594 or 633nm. Emission wavelengths (tuned with an AOTF) were specifically selected for each fluorochrome. Z-stacks were taken at numerous sites along each isolated lymphatic and throughout the lymphatic network in whole mount mesenteries from the first collecting lymphatics outside the intestinal wall all the way to the largest downstream collecting lymphatics near the nodal/antimesenteric border. Image reconstruction on the image stacks was performed using the Leica Confocal Software and ImageJ64. Image reconstruction and orthogonal viewing on the image stacks was performed using the Leica Confocal Software and ImageJ64. The negative controls for all experiments were produced and analyzed via same instrumental and image processing procedures.

Statistical analysis

All data are presented as mean values \pm standard error of the mean (SEM). The statistical significance of differences in mean values was analyzed with the unpaired, two-tailed Student's t test. P values less than 0.05 were considered significant. All statistical analyses were performed using Prism version 5.0 for Mac OS X (GraphPad).

Results

Lymphatic collecting vessels in adipose tissue associate with MHC II⁺ cells in multiple species

Fat pads typically surround LNs. When we mapped the lymphatic drainage system in mouse anterior subcutaneous adipose tissue by using optical projection tomography (Fig. 1, top row), we identified a cluster of lymphatic vessels at the origin of the fat pad near skin that drained into a lymph sinus (Fig. 1 top row, arrowhead). From this sinus, a lymphatic vessel corresponding to the afferent collecting vessel drained into the brachial LN and then departed the LN as an efferent lymphatic vessel (Fig. 1, top row, arrows). This collecting vessel was surrounded by smooth muscle actin-positive (SMA⁺) cells (Fig. 1, middle row, left image). Further associated with such lymphatic vessels were CD11c⁺ cells that were highly fluorescent cells in the CD11c-EYFP mouse strain (Fig. 1, middle row, right image). Cells with the highest levels of EYFP were DCs, not macrophages, since few adipose macrophages, identified as CD64⁺ MERTK⁺ cells (17) were fluorescent, in contrast to CD64⁻MERTK⁻CD11c⁺ MHC II⁺ DCs (Fig. 1, middle row, FACS plots). Intravital imaging analyses revealed that PAT CD11c-EYFP⁺ DCs that surrounded the collecting lymphatic vessels outside of the popliteal LN were highly motile and actively interacted with the exterior of these vessels, mobilizing along the lymphatic vessel wall, away from it, and within the adipose tissue (Fig. 1, lower row) (Supplemental Video 1).

We also examined rat mesenteric lymphatic vessels; these were surrounded by MHC II⁺ cells that retained association with the vessels even when they were isolated from the mesentery (Fig. 2). These rat prenodal mesenteric collecting lymphatics (average diameter 125 ± 21 μ m) were invested with numerous MHC II⁺ cells that covered 38 ± 6 % of the lymphatic wall surface area, scattered throughout all layers of the lymphatic wall (Fig. 2A-E). MHC II⁺ cells were also distributed throughout the nearby adipose and associated blood vessels (Fig. 2F-G).

Import of lymph-borne antigens and tracers into perinodal adipose tissue

Utilizing the mouse as an experimental model, we investigated whether adipose tissue DCs positioned near collecting lymphatic vessels would become charged with lymph-derived tracers that passed through collecting lymphatic vessels, given their proximity to these permeable vessels. Accordingly, we applied a contact sensitizer mixed with chemically reactive FITC to the skin surface of WT mice to assess whether DCs in PAT became FITC⁺. In this so-called “FITC painting” assay, DCs transport FITC-conjugated macromolecules from skin to LNs over an 18-h period, while additional FITC-conjugated molecules are carried in the lymph in soluble form and are readily visualized in the LN sinus and intranodal conduits (5, 15). Eighteen hours after applying FITC sensitizer to the skin surface, brightly fluorescent cells were found not only in draining lymph nodes but were also nested between adipocytes throughout the PAT (Fig. 3A-C). FITC⁺ cells recovered from the PAT were not limited to DCs. Instead, FITC was taken up by all types of cells in the adipose tissue (Fig. 3D). However, macrophages and DCs acquired significantly more FITC than other cells, such as eosinophils (Fig. 3D), likely due to their robust endocytic capacity.

Intradermal (i.d.) injection of recombinant E α GFP (16) also distributed broadly within PAT. Administration of fluorescent dextran as a tracer that readily drains through and therefore identifies lymphatic vessels (18) led to fluorescent cells in PAT and within the wall of collecting lymphatic vessels in only 7-10 minutes (Fig. 3E-F, Fig. S1). This rapid rate of labeling, far faster than DCs emigrate from the dermis to LNs (16), suggested that dextran was acquired locally by cells resident within PAT. Indeed, after FITC skin painting, more than half of the FITC⁺ cells appeared in PAT within 20 minutes, whereas migration of FITC⁺ DCs from skin was much slower (15, 19), thus eliminating the possibility that FITC⁺ cells in PAT emigrated to LNs first and then mobilized into PAT. Injection of labeled lymph-migrating DCs into the skin did not result in their appearance within PAT (unpublished observations). Taken together, these data indicate that acquisition of lymph-derived tracer by PAT cells was due to local sampling and uptake of material within lymph.

Accumulation of FITC⁺ cells in PAT after FITC skin painting depended upon a functional lymphatic network, because the number of FITC⁺ cells in PAT was more than 75% reduced in K14 VEGFR3-Ig mice, which lack skin lymphatic capillaries and cannot transport lymph to skin-draining LNs (14, 20) (Fig. 3G). Considering the importance of lymphatic vessels in promoting the distribution of antigen to PAT, we conducted further imaging studies to visualize the fate of lymph-borne tracers as they passed through the collecting lymphatics within PAT. Multi-photon microscopy of fixed specimens of PAT, prepared 12 h after E α GFP and 10 min after TRITC-dextran was injected into the mouse dermis, confirmed that antigen-acquiring cells were present within the wall of collecting lymphatic vessels. Cells that acquired TRITC-dextran within minutes after its administration were all E α GFP⁺, indicating that following uptake of E α GFP, these phagocytes remain local and were not stimulated to emigrate to LNs. (Fig. 4A-B, arrows in Fig. 4A). Lymphocytes (tracer-negative) within the lymph were clearly observed (Fig. 4B, arrows). While most of the phagocytic cells remained partially anchored within the collecting vessel wall or just outside of it, occasional GFP⁺ cytoplasmic projections appeared to extend into the lymphatic lumen (Fig. 4A-B).

Collectively, these data indicate that soluble components in lymph are shared with other cells within adipose tissue stromal vascular fraction in mice. To investigate whether this conclusion could be extended to other species, we injected FITC-conjugated bovine albumin directly into the rat lamina propria during intravital imaging. We observed cell bodies concentrating FITC-albumin along the borders of the mesenteric collecting vessel within 40 minutes (Fig. 4C-D), suggesting the presence of endocytic cells in the lymphatic wall able to sample lymph contents as observed in mice. Furthermore, we observed that PAT around peri-bronchial human LNs obtained from a cigarette smoker contained phagocytes filled with dark particulate matter that were likely derived from cigarette smoke (Fig. S2). Considering that such particulate matter is not found in circulating cells, the most probable mechanism behind its localization within PAT phagocytes is through emigration of phagocytes from lymph into PAT or, particularly, from lymph sampling. Collectively, the data from studies conducted in rodents suggest that lymph sampling leads to antigen deposition in PAT, a mechanism that could also be responsible for depositing foreign material in PAT in people.

Sampling of lymph-derived tracers by PAT DCs/macrophages leads to local inflammation and T cell recruitment during recall responses

After FITC skin painting (Fig. 5A), leukocytes, especially CD11c⁺ cells, were recruited to PAT. A similar response was evident after EaGFP was injected i.d. (Fig. 5A). Gene expression profiles in PAT showed increases in TNF α , IL-6, iNOS, TLR4, CCR2, MCP-1, and CD36 (Fig. 5B). To additionally assess whether lymph-sampled antigen might influence T cell accumulation in PAT in an antigen-dependent manner, we harvested CD45.1⁺CD4⁺ T cells in these draining LNs 4 days after FITC skin painting. These T cells, enriched in primed T cells specific for contact sensitizer antigens (21), or naïve T cells were transferred i.v. into non-immunized recipient CD45.2⁺ WT mice. Some of these WT recipients received no further manipulations, whereas other cohorts were immunized i.d. with EaGFP one day later, serving as an irrelevant antigen in this case, or by FITC skin painting, which set the stage for a recall response (21). Ear swelling tests indicated that transferred T cells supported the expected recall response (21) after FITC painting challenge (data not shown). Transferred reactive T cells and endogenous CD4⁺ T cells accumulated more in the PAT in recipient mice that challenged with FITC painting compared to no antigen or the irrelevant antigen-EaGFP treatment (Fig. 5C, D).

DCs from perinodal adipose tissue are recruited into inflamed lymph nodes

Although DCs emigrating to skin-draining LNs from lymphatic vessels are thought to arise from one of several skin DC subsets (22), the present findings indicating that lymph-derived antigens could be acquired by PAT DCs raised the possibility that PAT DCs might enter skin-draining LNs. To test this idea, we bypassed the dermal route of antigen administration, to avoid labeling dermal DCs, and injected EaGFP into PAT directly. Over the course of ~8 hours, the focal injection of EaGFP within PAT led to many individual EaGFP⁺ cells scattered throughout the surrounding adipose (Fig. 6A, B). Some of the labeled GFP⁺ cells migrated to the adjacent LN (Fig. 6A, right micrograph), peaking there between 12 and 36 h (Fig. 6B). These cells displayed Ea peptide on MHC II (I-A^b), as detected using the Y-Ae mAb (23) and co-expression of GFP (Fig. 6C). However, in concert with earlier studies, a small subset of cells with the highest levels of GFP and Y-Ae reactivity originated solely from the skin (16). Activation of TEa transgenic T cells, whose TCR specifically engages I-A^b complex with the Ea recognized by YAe mAb (12), occurred as efficiently for PAT-delivered EaGFP as it did for skin-delivered EaGFP (Fig. 6D). The rather slow time-frame (hours rather than minutes) of Y-Ae⁺ DCs appearing in the LN (Fig. 6B) and the requirement for CCR7 or its ligands (Fig. 6E) revealed that the appearance of Y-Ae⁺ DCs in the LN after EaGFP was administered to PAT was not the result of passive movement of EaGFP into the LN from the adipose tissue. Adoptive transfer of green fluorescent ex vivo-generated DCs into PAT led to a small fraction entering the LN, as is true with DCs are injected into skin. Sections through the PAT where the DCs were injected revealed a large collection of DCs at the site of injection with some DCs radiating away from the central site in the direction of the PAT collecting lymphatics (Fig. 6F). This pattern was not observed when CCR7^{-/-} DCs were injected (Fig. 6G), suggesting that the cells progressing toward the lymphatics from the injection site is CCR7-dependent. Indeed, we detected high levels of the CCR7 ligand CCL21 expressed by lymphatic collecting vessels (Fig. S3).

Our past work revealed that adjuvant-reactive LNs recruited more DCs as they undergo hypertrophy. In the PAT of mice receiving EαGFP i.d., however, we visualized fewer GFP⁺ cells in the spaces between adipocytes in mice treated with Complete Freund's Adjuvant (CFA) in one front forepaw 3 days earlier compared with control mice not receiving CFA (Fig. 7A, B). In the same samples, more GFP⁺ cells were observed in adjacent LNs, raising the possibility that inflamed, CFA-reactive LNs recruited more GFP⁺ cells from the PAT. Thus, we set out to address whether and to what extent reactive LNs may draw upon surrounding adipose tissue in recruiting antigen-bearing DCs. To aid in distinguishing lymph-migratory DCs that originated from skin versus PAT, we took advantage of an ancillary observation that skin painting with TRITC did not label PAT cells (negative data not shown) and did not lead to soluble TRITC⁺ molecules in LN sinus or conduits (Fig. 7B, C). Instead, it appeared that, TRITC, more reactive and hydrophobic than FITC, was carried to LNs only by lymph migratory DCs that become TRITC-labeled in skin (24), while it did not flow through lymph in soluble form that would enable access to LN sinus and conduits and sampling by PAT macrophages and DCs. By contrast, as noted earlier in this study and others (15, 16), FITC and EαGFP filled lymph node sinus and conduits and were sampled by PAT macrophages and DCs (Fig. 7C, D). We thus set up experiments in which we carried out FITC or TRITC skin painting in different cohorts of WT mice. Because we had earlier shown that adjuvant-reactive LNs could support increased DC migration during the ensuing LN hypertrophy (e.g., induction of DC migration induced from the scapular skin 3 days after CFA was injected in a front footpad) (10), we quantified the number of FITC⁺ or TRITC⁺ DCs in LNs of different cohorts of mice pretreated or not with CFA in one front footpad. The number of migratory FITC⁺ DCs in the CFA-reactive brachial LN doubled compared with the number in nonreactive LNs (Fig. 7E). However, no differences were observed in the number of TRITC⁺ DCs in nonreactive versus CFA-reactive LNs (Fig. 7E). This finding was consistent with the possibility that FITC⁺ DCs in PAT, lacking TRITC⁺ counterparts in PAT following TRITC painting, might be a key source of migratory DCs to enter CFA-reactive LNs.

To pursue this possibility further and quantify PAT-derived and skin-derived DCs simultaneously, we injected EαGFP i.d. to permit labeling of PAT DCs 4 h before applying TRITC to the skin of the same mice in the area that drains to the same brachial LN. When we harvested the LNs 18 h later, we found 3 populations of migratory DCs (CD11c^{hi}MHCII^{hi}) in the draining LN: TRITC⁺EαGFP⁺, TRITC⁺EαGFP⁻, and much more rarely TRITC⁻EαGFP⁺, with only the latter potentially originating from PAT (Fig. 7F). By contrast, when this experiment was performed in mice with CFA-reactive LNs, TRITC⁻EαGFP⁺ cells were the only population to substantially increase and they increased sufficiently greatly (more than 3 fold) to comprise approximately one-third of the antigen-labeled DCs in such LNs (Fig. 7F). When we repeated this experiment but instead injected EαGFP on the contralateral side of the mouse to make sure that TRITC⁻EαGFP⁺ DCs did not arise from systemic spread and uptake of soluble EαGFP in DCs or DC precursors that might enter the LN through the high endothelial venules, we found no EαGFP⁺ DCs in CFA-reactive contralateral LN (negative result not shown). Thus, these data collectively suggest that PAT DCs emigrate to LNs, especially under conditions of LN hypertrophy, where they contribute substantially to the overall pool of migratory DCs.

Discussion

Perinodal adipose tissue colocalizes with LNs throughout the body, and is a conserved feature of mammalian anatomy (25). The immune function of this fat depot and its relationship with local LNs is not known. The fat pads around LNs extend beyond the nodes along the collecting lymphatic vessels that feed into (afferent) and run out of (efferent) LNs, such that collecting lymphatic vessels are most closely associated with PAT. We show here that the inherent permeability of collecting lymphatic vessels is sufficient to broadcast antigens, passing within lymph to LNs, throughout PAT. The delivery of soluble antigens, such as FITC-conjugated endogenous proteins and E α -GFP, is likely a passive consequence of the permeability of collecting lymphatic vessels. This process exposes a large community of endocytic and phagocytic cells, particularly DCs and macrophages, to antigens that would otherwise be unavailable to them.

It is also possible that DCs or macrophages can actively sample the contents of the lymphatic lumen. DCs, in particular, were observed by intravital imaging to intimately interact with collecting lymphatic vessels along with images displaying pseudopod-like projections in the lumen. Moreover, our findings of particulate matter in PAT around human bronchial LNs is consistent with this possibility, though anecdotal. Active lymph sampling by adipose DCs/macrophages could explain the accumulation of micro-organisms, such as *Mycobacterium tuberculosis*, in adipose tissue (26).

Our findings suggest persistent inflammation within fat depots is caused, at least in part, by disease-promoting antigens that course through the lymph in collecting lymphatic vessels. Our observation that fat around collecting lymphatic vessels can accumulate T cells with specificity to antigens derived from lymph contents, support the notion that changes in the adipose tissue T cell compartment associated with disease might likewise occur in response to antigens that originate from lymph. In this context, it is interesting to consider connections to adipose tissue inflammation in the context of obesity, where macrophages, DCs, and T cells appear to play a critical role (27-29). Furthermore, mesenteric adipose tissue would be expected to be exposed to and accumulate lymph-derived molecules from the intestine, whereas PAT would acquire antigens from a variety of organs drained by the relevant LNs.

At these sites, signals derived from lymph may impact the adipocyte environment, perhaps to promote adipose growth (9) through crosstalk with pre-adipocytes themselves located in walls of nearby vessels (30). Many PAT in mice and man correspond with depots containing beige adipocytes (31-35), which are capable of assuming a fat-storing white adipocyte phenotype or a fuel-demanding thermogenic brown fat. That macrophages have been shown to impact the activity of brown fat raises the possibility that factors in lymph that condition macrophages may in turn affect adipocyte differentiation (36). Thus, the present findings support the need for future studies of immunological diseases in the intestine and beyond, including Crohn's disease or HIV known to be linked in still obscure ways to changes in adipose tissue, lymphatic vessels, or both (25, 37) (38-41).

We have emphasized the uptake of antigens as a component of lymph capable of being processed by phagocytes. However, we recognize that the broadcast and sampling of endogenous macromolecules from lymph might also transmit to fat information about the physiological status of adjacent organs drained by a common lymphatic vasculature. An example might be the breakdown of hyaluronan within tissues in response to tissue injury (42). The receptor LYVE-1 on lymphatic capillaries in organs binds hyaluronan, but collecting lymphatic vessels do not express it (43). In scenarios wherein hyaluronan breaks down to a sufficient degree to enter lymph and not be cleared in the lymphatic capillary before reaching the collecting lymphatic vessel, permeable collecting lymphatic vessels will provide PAT DCs and macrophages with a signal via hyaluronan fragments. As these promote DC migration to LNs (44), among other defense and healing reactions (42), the adipose tissue may become a critical source of signals that affect the response to injury, as well as a source of migratory DCs to enter the draining lymph.

It is clear that enhancing or dampening the number of lymph-migratory DCs bearing antigen impacts the quality and character of an ongoing immune response (19, 44, 45). We have had a long-standing interest in how the LN coordinates signals to undergo hypertrophy during a vigorous immune response and still maintain ideal ratios of lymphocytes, which enter often through HEV, to antigen-bearing DCs coming from lymph (10). We show here that one of the consequences of charging PAT DCs with antigens acquired through permeable collecting lymphatic vessels is the supply to the LN of a reserve of antigen-bearing DCs for the hypertrophic LN. Thus, in addition to the wide array of different DC subtypes now described in the parenchyma of organs like skin (22), the DC compartment capable of acquiring and transporting antigens to LNs must be expanded to consider DC populations beyond the organ residing within the PAT.

Supplementary Material

Refer to Web version on PubMed Central for supplementary material.

Acknowledgments

We thank Marc Jenkins (University of Minnesota) for the gift of plasmids encoding E_oGFP and E_oCherry, Kari Alitalo (University of Helsinki) for the K14-VEGFR3 Ig transgenic mice, Jonathan Bromberg for sharing TCR-transgenic TEa mice, and Jens Stein (University of Bern) for protocols in whole-mount staining of the LN and adipose tissue. We are also grateful for the expert assistance we received at several Shared Resource Facilities (imaging, flow cytometry, quantitative PCR) at Mount Sinai School of Medicine, at the Integrated Microscopy Imaging Lab at the Texas A&M Health Science Center, and at the Rockefeller University Bio-Imaging Resource Center.

Grant Support: This research was funded by an Established Investigator Award from the American Heart Association, NIH AI 049653 grant, a Nutrition & Obesity Research Center Pilot and Feasibility subaward to NIH P30 DK05341, and an Innovation Award from the Rainin Foundation to GJR, NIH HL084312 to GJR and MAS, NIH AI055037 to MD, and NIH HL075199, HL70308 and HL085659 to DCZ, NIH AG030578 to AAG, NIH AI082982 to RJM, and an NIH supplement to CJ linked to NIH grant HL081151 to Peter Henson (National Jewish Health, Denver). Imaging studies conducted at the Rockefeller University were supported by the Empire State Stem Cell Fund through NYSDOH Contract #C023046. Opinions expressed here are solely those of the author and do not necessarily reflect those of the Empire State Stem Cell Fund, the NYSDOH, or the State of NY. Current addresses are ELK, Immunology Program, Benaroya Research Institute, Seattle, WA; EB, Scientific Equipment Group, Olympus Corporation of the Americas; GV, Whitehead Institute for Biomedical Research, Cambridge, MA; AMP, Quintiles, Livingston, The United Kingdom.

References

1. Schmid-Schonbein GW. Microlymphatics and lymph flow. *Physiol Rev.* 1990; 70:987–1028. [PubMed: 2217560]
2. Baluk P, Fuxe J, Hashizume H, Romano T, Lashnits E, Butz S, Vestweber D, Corada M, Molendini C, Dejana E, McDonald DM. Functionally specialized junctions between endothelial cells of lymphatic vessels. *The Journal of experimental medicine.* 2007; 204:2349–2362. [PubMed: 17846148]
3. Muthuchamy M, Zawieja D. Molecular regulation of lymphatic contractility. *Ann N Y Acad Sci.* 2008; 1131:89–99. [PubMed: 18519962]
4. Scallan JP, Huxley VH. In vivo determination of collecting lymphatic vessel permeability to albumin: a role for lymphatics in exchange. *The Journal of physiology.* 2010; 588:243–254. [PubMed: 19917564]
5. Randolph GJ, Angeli V, Swartz MA. Dendritic-cell trafficking to lymph nodes through lymphatic vessels. *Nature reviews Immunology.* 2005; 5:617–628.
6. Pflücke H, Sixt M. Preformed portals facilitate dendritic cell entry into afferent lymphatic vessels. *The Journal of experimental medicine.* 2009; 206:2925–2935. [PubMed: 19995949]
7. Harvey NL. The link between lymphatic function and adipose biology. *Ann N Y Acad Sci.* 2008; 1131:82–88. [PubMed: 18519961]
8. Mayerson HS. On Lymph and Lymphatics. *Circulation.* 1963; 28:839–842. [PubMed: 14079186]
9. Harvey NL, Srinivasan RS, Dillard ME, Johnson NC, Witte MH, Boyd K, Sleeman MW, Oliver G. Lymphatic vascular defects promoted by Prox1 haploinsufficiency cause adult-onset obesity. *Nature genetics.* 2005; 37:1072–1081. [PubMed: 16170315]
10. Angeli V, Ginhoux F, Llodra J, Quemeneur L, Frenette PS, Skobe M, Jessberger R, Merad M, Randolph GJ. B cell-driven lymphangiogenesis in inflamed lymph nodes enhances dendritic cell mobilization. *Immunity.* 2006; 24:203–215. [PubMed: 16473832]
11. Gunn MD, Kyuwa S, Tam C, Kakiuchi T, Matsuzawa A, Williams LT, Nakano H. Mice lacking expression of secondary lymphoid organ chemokine have defects in lymphocyte homing and dendritic cell localization. *J Exp Med.* 1999; 189:451–460. [PubMed: 9927507]
12. Grubin CE, Kovats S, deRoos P, Rudensky AY. Deficient positive selection of CD4 T cells in mice displaying altered repertoires of MHC class II-bound self-peptides. *Immunity.* 1997; 7:197–208. [PubMed: 9285405]
13. Lindquist RL, Shakhar G, Dudziak D, Wardemann H, Eisenreich T, Dustin ML, Nussenzweig MC. Visualizing dendritic cell networks in vivo. *Nature immunology.* 2004; 5:1243–1250. [PubMed: 15543150]
14. Makinen T, Jussila L, Veikkola T, Karpanen T, Kettunen MI, Pulkkanen KJ, Kauppinen R, Jackson DG, Kubo H, Nishikawa S, Yla-Herttuala S, Alitalo K. Inhibition of lymphangiogenesis with resulting lymphedema in transgenic mice expressing soluble VEGF receptor-3. *Nature medicine.* 2001; 7:199–205.
15. Robbiani DF, Finch RA, Jager D, Muller WA, Sartorelli AC, Randolph GJ. The leukotriene C(4) transporter MRP1 regulates CCL19 (MIP-3beta, ELC)- dependent mobilization of dendritic cells to lymph nodes [In Process Citation]. *Cell.* 2000; 103:757–768. [PubMed: 11114332]
16. Itano AA, McSorley SJ, Reinhardt RL, Ehst BD, Ingulli E, Rudensky AY, Jenkins MK. Distinct dendritic cell populations sequentially present antigen to CD4 T cells and stimulate different aspects of cell-mediated immunity. *Immunity.* 2003; 19:47–57. [PubMed: 12871638]
17. Gautier EL, Shay T, Miller J, Greter M, Jakubzick C, Ivanov S, Helft J, Chow A, Elpek KG, Gordonov S, Mazloom AR, Ma'ayan A, Chua WJ, Hansen TH, Turley SJ, Merad M, Randolph GJ, C. Immunological Genome. Gene-expression profiles and transcriptional regulatory pathways that underlie the identity and diversity of mouse tissue macrophages. *Nature immunology.* 2012; 13:1118–1128. [PubMed: 23023392]
18. Swartz MA, Berk DA, Jain RK. Transport in lymphatic capillaries. I. Macroscopic measurements using residence time distribution theory. *Am J Physiol.* 1996; 270:H324–329. [PubMed: 8769768]
19. Allan RS, Waithman J, Bedoui S, Jones CM, Villadangos JA, Zhan Y, Lew AM, Shortman K, Heath WR, Carbone FR. Migratory dendritic cells transfer antigen to a lymph node-resident

- dendritic cell population for efficient CTL priming. *Immunity*. 2006; 25:153–162. [PubMed: 16860764]
20. Rutkowski JM, Markhus CE, Gyenge CC, Alitalo K, Wiig H, Swartz MA. Dermal collagen and lipid deposition correlate with tissue swelling and hydraulic conductivity in murine primary lymphedema. *The American journal of pathology*. 2010; 176:1122–1129. [PubMed: 20110415]
 21. Macatonia SE, Knight SC. Dendritic cells and T cells transfer sensitization for delayed-type hypersensitivity after skin painting with contact sensitizer. *Immunology*. 1989; 66:96–99. [PubMed: 15493269]
 22. Henri S, Williams M, Poulin LF, Tamoutounour S, Ardouin L, Dalod M, Malissen B. Disentangling the complexity of the skin dendritic cell network. *Immunology and cell biology*. 2010; 88:366–375. [PubMed: 20231850]
 23. Rudensky A, Rath S, Preston-Hurlburt P, Murphy DB, Janeway CA Jr. On the complexity of self. *Nature*. 1991; 353:660–662. [PubMed: 1656278]
 24. Jakubzick C, Bogunovic M, Bonito AJ, Kuan EL, Merad M, Randolph GJ. Lymph-migrating, tissue-derived dendritic cells are minor constituents within steady-state lymph nodes. *The Journal of experimental medicine*. 2008; 205:2839–2850. [PubMed: 18981237]
 25. Knight SC. Specialized perinodal fat fuels and fashions immunity. *Immunity*. 2008; 28:135–138. [PubMed: 18275823]
 26. Neyrolles O, Hernandez-Pando R, Pietri-Rouxel F, Fornes P, Tailleux L, Barrios Payan JA, Pivert E, Bordat Y, Aguilar D, Prevost MC, Petit C, Gicquel B. Is adipose tissue a place for *Mycobacterium tuberculosis* persistence? *PloS one*. 2006; 1:e43. [PubMed: 17183672]
 27. Nishimura S, Manabe I, Nagasaki M, Eto K, Yamashita H, Ohsugi M, Otsu M, Hara K, Ueki K, Sugiura S, Yoshimura K, Kadowaki T, Nagai R. CD8+ effector T cells contribute to macrophage recruitment and adipose tissue inflammation in obesity. *Nature medicine*. 2009; 15:914–920.
 28. Feuerer M, Herrero L, Cipolletta D, Naaz A, Wong J, Nayer A, Lee J, Goldfine AB, Benoist C, Shoelson S, Mathis D. Lean, but not obese, fat is enriched for a unique population of regulatory T cells that affect metabolic parameters. *Nature medicine*. 2009; 15:930–939.
 29. Winer S, Chan Y, Paltser G, Truong D, Tsui H, Bahrami J, Dorfman R, Wang Y, Zielenski J, Mastronardi F, Maezawa Y, Drucker DJ, Engleman E, Winer D, Dosch HM. Normalization of obesity-associated insulin resistance through immunotherapy. *Nature medicine*. 2009; 15:921–929.
 30. Tang W, Zeve D, Suh JM, Bosnakovski D, Kyba M, Hammer RE, Tallquist MD, Graff JM. White fat progenitor cells reside in the adipose vasculature. *Science*. 2008; 322:583–586. [PubMed: 18801968]
 31. Vitali A, Murano I, Zingaretti MC, Frontini A, Ricquier D, Cinti S. The adipose organ of obesity-prone C57BL/6J mice is composed of mixed white and brown adipocytes. *Journal of lipid research*. 2012; 53:619–629. [PubMed: 22271685]
 32. Cypess AM, Lehman S, Williams G, Tal I, Rodman D, Goldfine AB, Kuo FC, Palmer EL, Tseng YH, Doria A, Kolodny GM, Kahn CR. Identification and importance of brown adipose tissue in adult humans. *N Engl J Med*. 2009; 360:1509–1517. [PubMed: 19357406]
 33. van Marken Lichtenbelt WD, Vanhommerig JW, Smulders NM, Drossaerts JM, Kemerink GJ, Bouvy ND, Schrauwen P, Teule GJ. Cold-activated brown adipose tissue in healthy men. *N Engl J Med*. 2009; 360:1500–1508. [PubMed: 19357405]
 34. Saito M, Okamatsu-Ogura Y, Matsushita M, Watanabe K, Yoneshiro T, Nio-Kobayashi J, Iwanaga T, Miyagawa M, Kameya T, Nakada K, Kawai Y, Tsujisaki M. High incidence of metabolically active brown adipose tissue in healthy adult humans: effects of cold exposure and adiposity. *Diabetes*. 2009; 58:1526–1531. [PubMed: 19401428]
 35. Jespersen NZ, Larsen TJ, Peijs L, Dagaard S, Homoe P, Loft A, de Jong J, Mathur N, Cannon B, Nedergaard J, Pedersen BK, Moller K, Scheele C. A classical brown adipose tissue mRNA signature partly overlaps with brite in the supraclavicular region of adult humans. *Cell metabolism*. 2013; 17:798–805. [PubMed: 23663743]
 36. Nguyen KD, Qiu Y, Cui X, Goh YP, Mwangi J, David T, Mukundan L, Brombacher F, Locksley RM, Chawla A. Alternatively activated macrophages produce catecholamines to sustain adaptive thermogenesis. *Nature*. 2011; 480:104–108. [PubMed: 22101429]

37. Van Kruiningen HJ, Colombel JF. The forgotten role of lymphangitis in Crohn's disease. *Gut*. 2008; 57:1–4. [PubMed: 18094195]
38. Lake JE, Currier JS. Metabolic disease in HIV infection. *The Lancet infectious diseases*. 2013; 13:964–975. [PubMed: 24156897]
39. Agarwal N, Iyer D, Patel SG, Sekhar RV, Phillips TM, Schubert U, Oplt T, Buras ED, Samson SL, Couturier J, Lewis DE, Rodriguez-Barradas MC, Jahoor F, Kino T, Kopp JB, Balasubramanyam A. HIV-1 Vpr induces adipose dysfunction in vivo through reciprocal effects on PPAR/GR co-regulation. *Science translational medicine*. 2013; 5:213ra164.
40. Guaraldi G, Luzi K, Bellistri GM, Zona S, Domingues da Silva AR, Bai F, Garlassi E, Marchetti G, Capeau J, Monforte A. CD8 T-cell activation is associated with lipodystrophy and visceral fat accumulation in antiretroviral therapy-treated virologically suppressed HIV-infected patients. *Journal of acquired immune deficiency syndromes*. 2013; 64:360–366. [PubMed: 24129368]
41. Shikuma CM, Gangcuangco LM, Killebrew DA, Libutti DE, Chow DC, Nakamoto BK, Liang CY, Milne CI, Ndhlovu LC, Barbour JD, Shiramizu BT, Gerschenson M. The Role of HIV and Monocytes/Macrophages in Adipose Tissue Biology. *Journal of acquired immune deficiency syndromes*. 2014; 65:151–159. [PubMed: 24091690]
42. Jackson DG. Immunological functions of hyaluronan and its receptors in the lymphatics. *Immunological reviews*. 2009; 230:216–231. [PubMed: 19594639]
43. Makinen T, Adams RH, Bailey J, Lu Q, Ziemiecki A, Alitalo K, Klein R, Wilkinson GA. PDZ interaction site in ephrinB2 is required for the remodeling of lymphatic vasculature. *Genes & development*. 2005; 19:397–410. [PubMed: 15687262]
44. Muto J, Morioka Y, Yamasaki K, Kim M, Garcia A, Carlin AF, Varki A, Gallo RL. Hyaluronan digestion controls DC migration from the skin. *The Journal of clinical investigation*. 2014
45. MartIn-Fontecha A, Sebastiani S, Hopken UE, Ugucioni M, Lipp M, Lanzavecchia A, Sallusto F. Regulation of dendritic cell migration to the draining lymph node: impact on T lymphocyte traffic and priming. *The Journal of experimental medicine*. 2003; 198:615–621. [PubMed: 12925677]

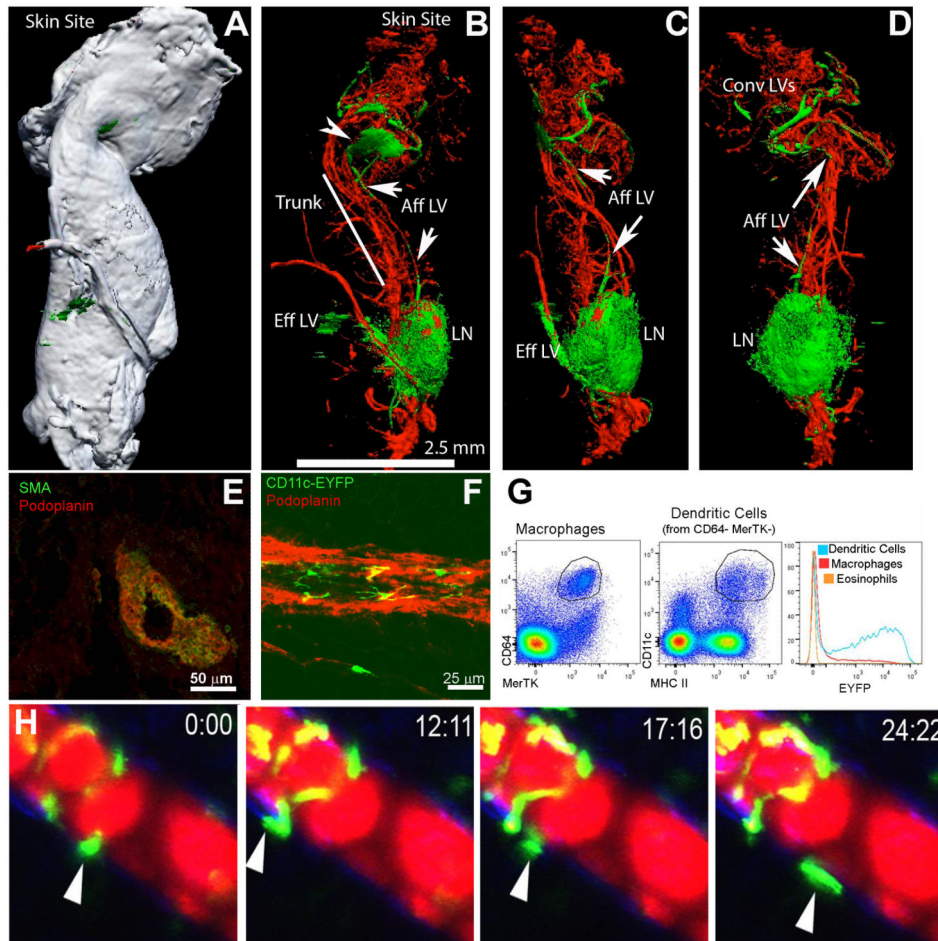


Figure 1. Collecting lymphatic vessels in PAT and their interactions with DCs

A-D, Optical projection tomography of the brachial LN remove from scapular skin depicts the gross relationship between this LN and the surrounding lymphatic vessels and PAT. Green, lymphatic tracer; red, blood tracer. White color in Panel A shows the contour of PAT around LNs, with Panels B-D showing internal fluorescence in orientations identical to Panel A or partially rotated (B-C). Convergent lymphatics (Conv LVs) near the skin pool at a lymphatic sinus (arrowhead, B) and then a single major afferent lymphatic (Aff LV, arrows) moves along the trunk of the PAT to the LN, with the efferent vessel following the blood supply emerging from the LN hilum. E) Cross-section of the afferent lymphatic in the PAT trunk showing smooth muscle actin and podoplanin costaining. F) CD11c-YFP⁺ cells visualized outside of podoplanin⁺ lymphatic vessels in PAT. G) Gating on macrophages, DCs, or eosinophils in PAT shows that only DCs are YFP⁺ in CD11c-YFP mice. H) Time-lapse images of CD11c-YFP DCs around popliteal PAT following injection of Evan's blue dye (fluoresces red) in the rear footpad. All images shown are representative of 2 independent experiments performed in triplicate.

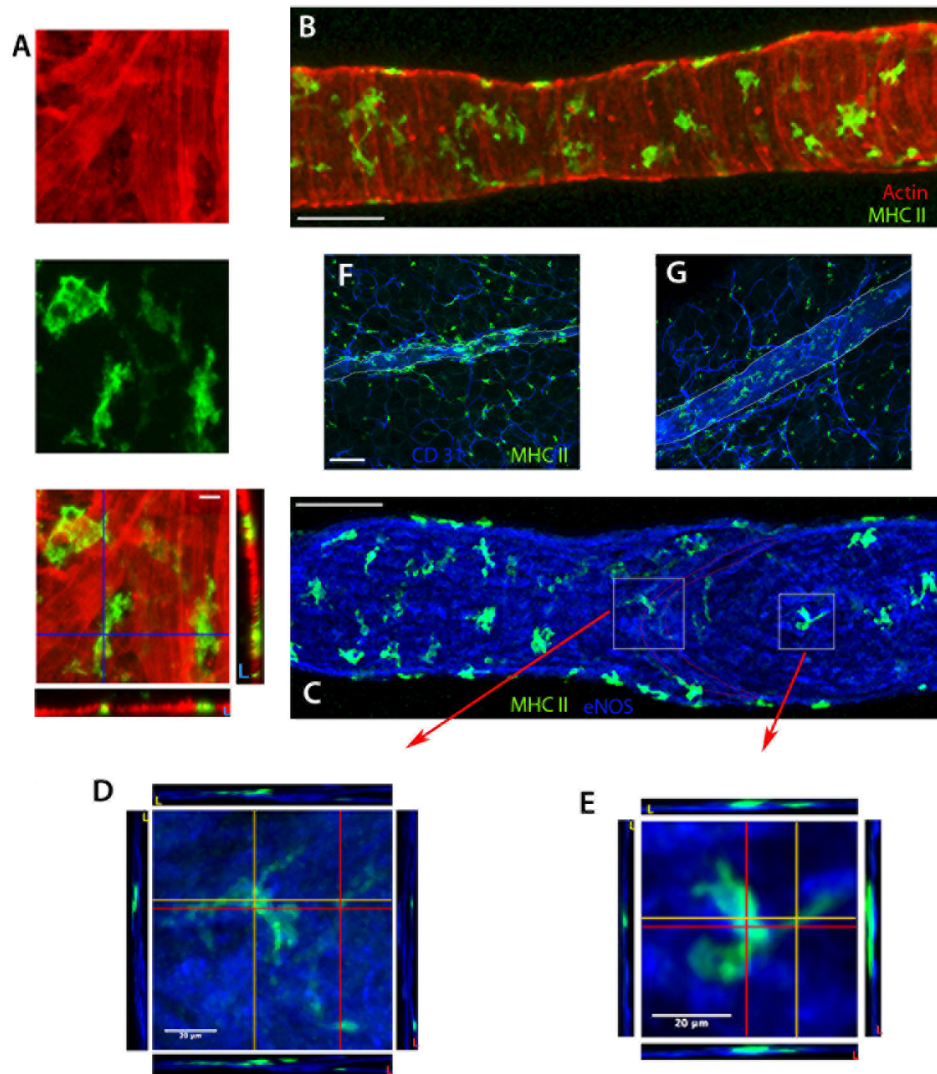


Figure 2. MHC II⁺ cells within the wall of rat mesenteric collecting lymphatic vessels
 A-E) Z-axis projections of isolated, rat mesenteric collecting lymphatics stained for MHC II (green), α -smooth muscle actin (red) and eNOS (blue). Panels A (higher magnification) and B (lower magnification) show the localization of MHC II⁺ cells within the α - smooth muscle actin-positive lymphatic wall. Panels C-E reveal MHC II⁺ cells within the lymphatic wall, here co-stained for eNOS. Boxed insets in Panel C show the downstream edge of valve leaflets, with Panels D and E are higher magnification images from C (white squares) depicting the orthogonal cross-sectional views at the locations marked by the red and orange lines revealing that the macrophages bodies are primarily abluminal to the lymphatic endothelial cells. F-G) Z axis projections of rat mesenteric whole-mount preparations stained for MHC II⁺ cells (green) and endothelium by CD31 (blue). The collecting lymphatic wall is indicated by thin white lines. Panel F is a tissue section with an upstream lymphangion within the adipose near the gut, while G is a tissue section with a lymphangion within the adipose downstream of F, in the same lymphatic network near the lymph node.

Scale bar is 100 μm unless otherwise indicated. Data in these panels are derived from 2-8 experiments, with n = 2 replicates per condition.

Author Manuscript

Author Manuscript

Author Manuscript

Author Manuscript

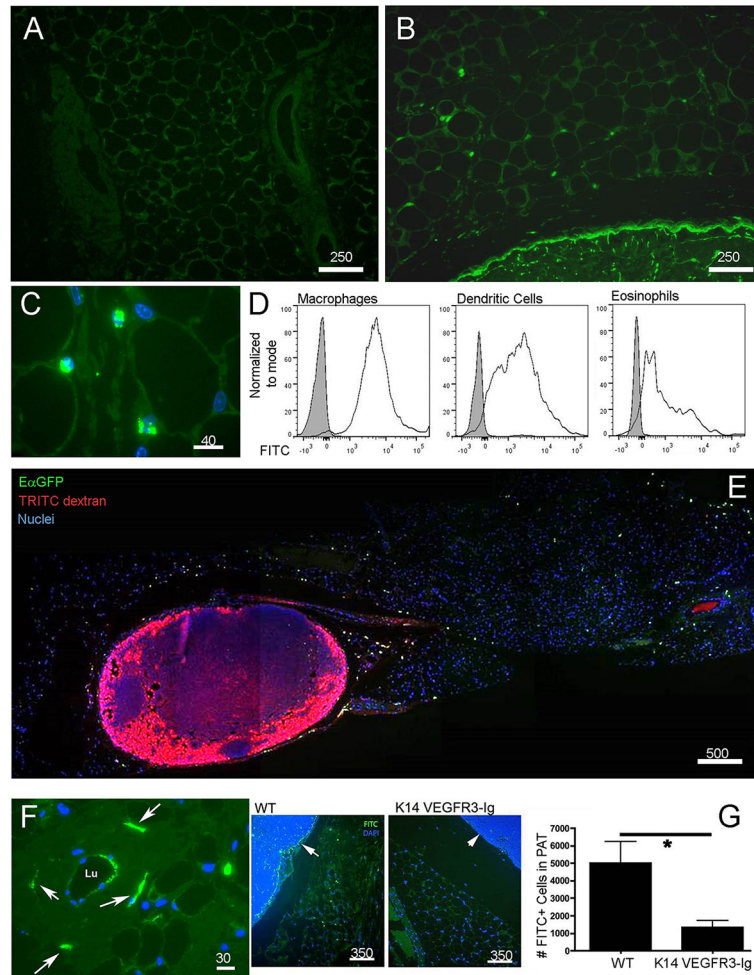


Figure 3. Passage of soluble antigens from collecting lymphatic vessels to adipose tissue phagocytes

A, B) Low power cross-sections depicting PAT outside of the brachial LN 18 h after application to the skin surface of a contact sensitizer containing FITC (green) as a hapten (Panel B) compared to the same PAT without FITC painting in Panel A. C) Higher power view of FITC⁺ cells (green) in PAT as in B. D) Flow cytometric analysis to quantify FITC uptake 18 h after FITC skin painting in DCs (CD45⁺CD11c⁺MHCII⁺MERTK⁻CD64⁻), macrophages (CD45⁺MERTK⁺CD64⁺), and eosinophils (CD45⁺MERTK⁻SiglecF⁺). E) Low power tile-reconstructed view of a cross-section of PAT and brachial LN 20 h after EαGFP (green) was administered intradermally (i.d.) and 10 min. after 70 kDa TRITC-dextran (red) was injected i.d. F) Higher power view of PAT cross-section 10 min after FITC-dextran (green) i.d. shows a collecting vessel wall with dextran-enriched cells nearby (white arrow). G) Mice with defective lymphatics resulting from expression of VEGFR3-Ig from the K14 promoter and their littermate WT controls were subjected to FITC skin painting for 18 h. FITC⁺ cells in PAT cross-sections were counted (n=3 per group). Arrows point to the subcapsular sinus in each strain. Number above scale bars corresponds to number of microns. All images shown were representative of at least 3 animals per group.

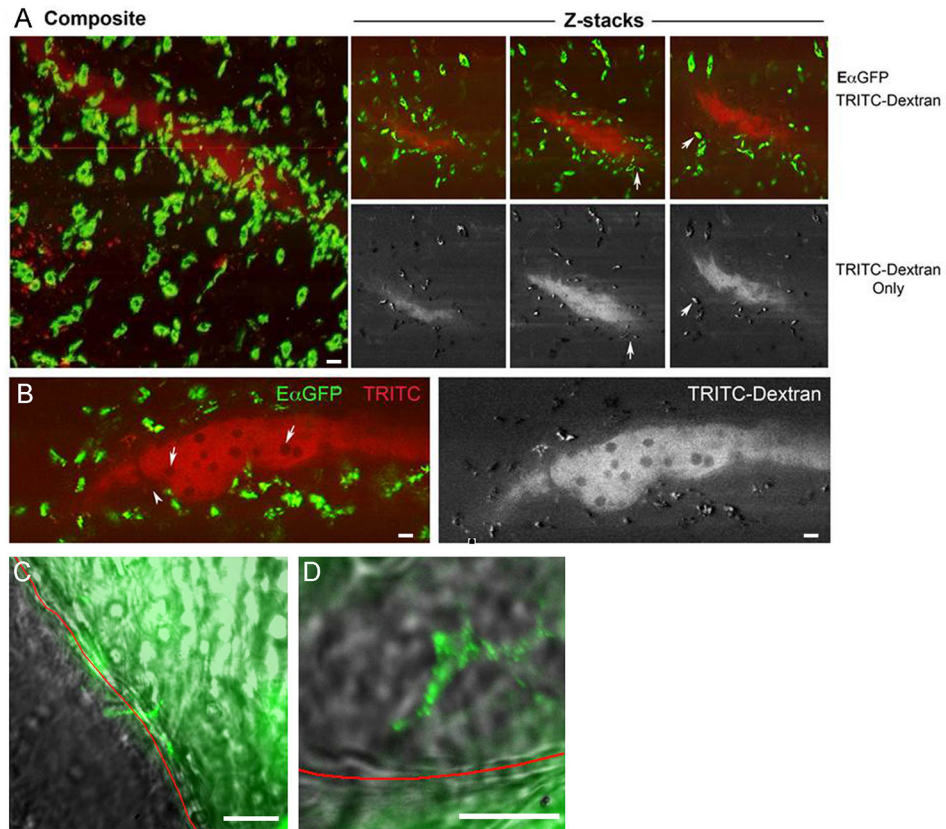


Figure 4. Endocytic acquisition of tracers by phagocytes in PAT

A) Z stacks acquired from multiphoton microscopy on fixed PAT obtained from mice injected with E α GFP i.d. 12 h previously and then injected with TRITC-dextran (red) 10 min. prior to euthanasia. Red color identifies lymphatic lumen filled with TRITC dextran and cells acquiring TRITC dextran. Left panel, maximum projection of z-stacks compiled through 200 μ m of PAT. Right panels show 3 individual z stack images; upper ones demonstrate both green (FITC) and red (TRITC) channels. Lower ones depict only the TRITC channel (in white contrast). Arrows indicate cells that are both FITC⁺ and TRITC. B) Higher power view of z-stack image. Dark circles (arrows) in the lumen are poorly endocytic T cells. Arrowhead indicates cells that took up E α GFP and extend pseudopods into the lumen. C, D) FITC-BSA was injected in the exteriorized rat mesentery. Live confocal imaging of the fluorescent tracer as it passed through mesenteric collecting vessel s began immediately. Red line delineates the border of the lymphatic vessel with surrounding adipose tissue and the lymphatic lumen as marked. Arrows depict cell bodies that appear to concentrate the tracer. Live imaging precluded immunostaining to identify these cells. Scale bar in all images is 30 μ m. Data in each panel are representative of 2-3 independent experiments.

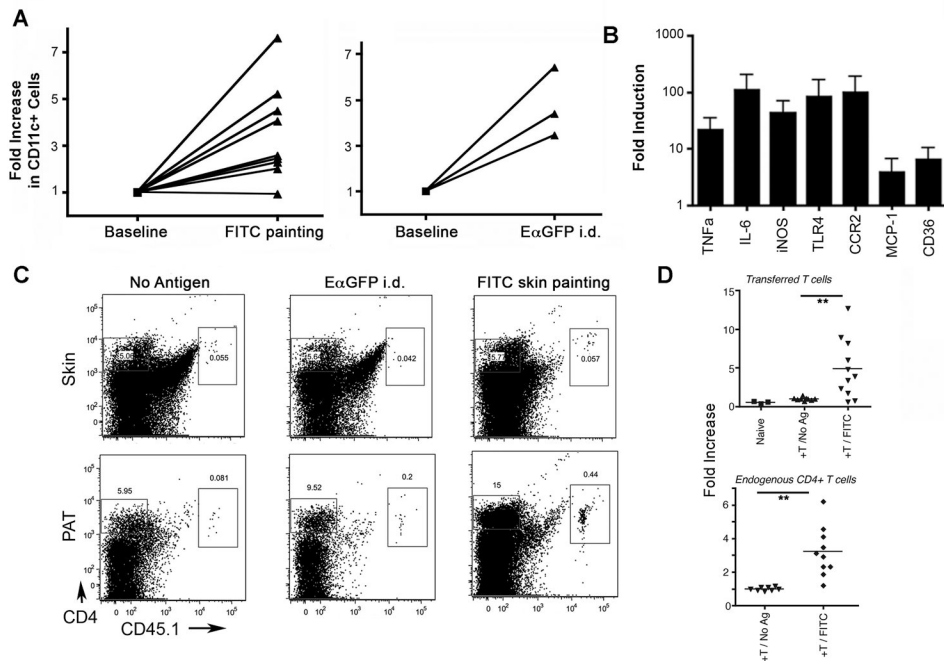


Figure 5. Inflammatory responses in PAT after skin immunization

A) Each line in the graphs represents an independent experiment in which the fold-increase in PAT CD11c⁺ inflammatory cells was measured 18 h after epicutaneous application of FITC sensitizer or 18 h after EαGFP was injected i.d. B) Quantitative PCR analysis to determine fold increase in mRNA for inflammatory mediators and key adipose-derived cytokines- TNFα, IL-6, iNOS, TLR4, CCR2, MCP-1, and CD36, 12 h after application of FITC sensitizer to skin. C, D) CD4⁺ T cells were purified from either naïve LNs (+Naïve T) or reactive LNs (+T) of CD45.1⁺ WT mice 4 days after FITC skin painting and transferred into CD45.2⁺ WT mice. These recipients were challenged 5 h later with FITC painting or an irrelevant antigen to which they were naïve (EαGFP) or not challenged (No Antigen). Accumulation of transferred CD45.1⁺ CD4⁺ and endogenous CD45.2⁺ CD4⁺ T cells in the site of skin challenge or the associated PAT was analyzed ~36 h after challenge. Panel C shows the representative FACS plots of transferred T cells in skin or in PATs. Panel D charts the number of T cells accumulated in PAT of antigen challenged mice, expressed as fold-increase over the number of accumulated in the absence of antigen challenge. **, P < 0.01. All data were obtained from at least 2 independent experiments with more than 3 replicates per group in each experiment.

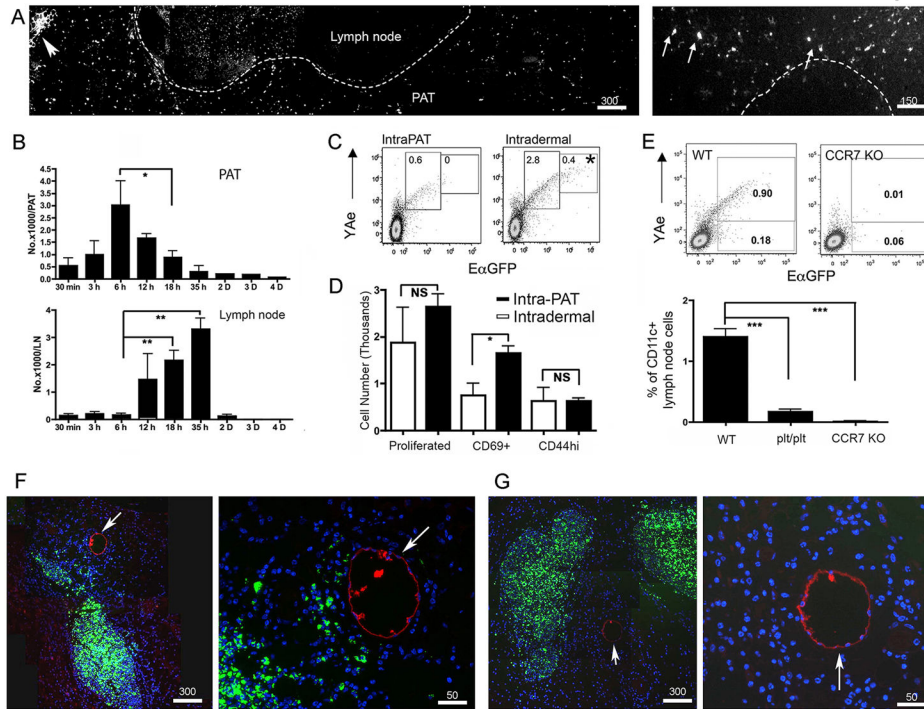


Figure 6. DCs from PAT use CCR7 to home to adjacent LNs

A) EαGFP or EαCherry (20 μg in 2 μl) was injected (intraPAT) into two sites of mouse PAT around brachial LN. The distribution of EαGFP⁺ cells was analyzed 18 h later. Arrowhead, injection site; arrow, EαGFP⁺ cells in LN. Dashed line delineates border of PAT and brachial LN on left, and the border of the LN B cell and T cell zone on right. B) Total number of EαGFP⁺YAe⁺CD11c⁺CD45⁺ cells in PAT and LN over time following intraPAT EαGFP delivery. At least 3 mice per time point were used. C) EαGFP and YAe expression in CD11c⁺ cells from brachial LNs 18 h after intraPAT (20 μg) or i.d. (40 μg in scapular skin) delivery of EαGFP. D) Sorted, CFSE-labeled naïve Tea transgenic T cells were transferred i.v. into naïve recipient mice that 24 h later received intraPAT (20 μg/ PAT, solid bars) or i.d. (40 μg in upper scapular skin, open bars) injection of EαCherry. Total proliferated TEa⁺CD4⁺CFSE^{lo} T cells and CD69⁺ or CD44⁺ proportions in draining LNs were quantified. E) WT, CCR7 KO, or plt/plt mice received intraPAT EαGFP. After 18 h, percent EαGFP⁺YAe⁺ cells among CD11c⁺ LN cells was analyzed. F, G) Fluorescent bead-labeled bone marrow-derived DCs (green) from WT (F) or CCR7 KO (G) mice were injected directly into WT mice PAT for 24 h; 10 min before euthanasia, TRITC-dextran (red) was delivered i.d. to label lymphatics (white arrows). Scale bars in microns. Data show mean ± SEM. *, P < 0.05; **, P < 0.01; ***, P < 0.001. NS means non-statistical different. (A), and (C)-(G) were obtained from 3 independent experiments with at least 3 replicates per group in each experiment.

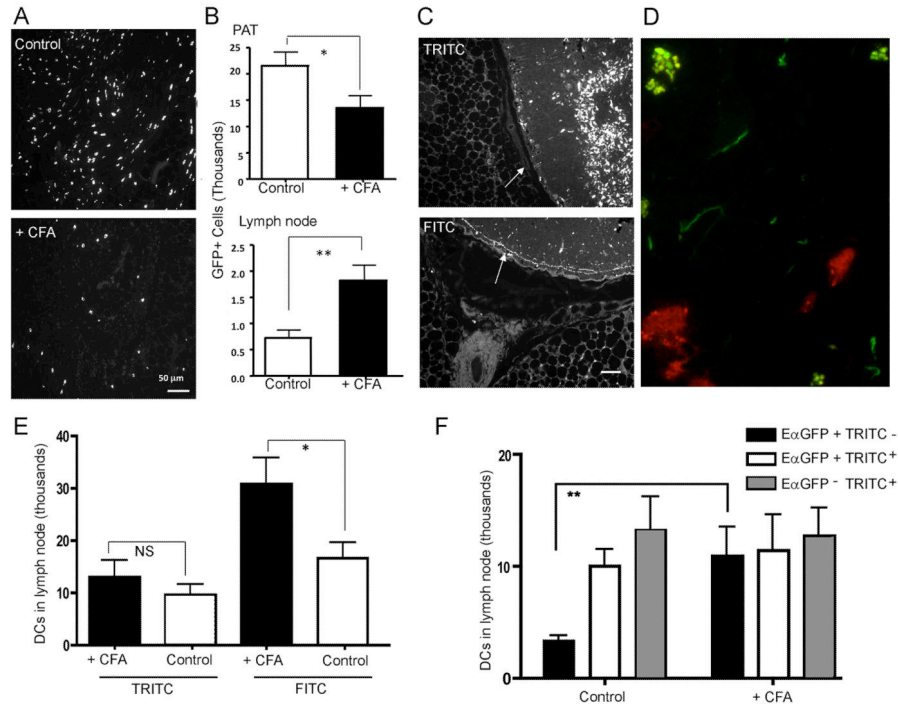


Figure 7. Inflammation increases mobilization of DCs from PAT to the adjacent LN
 Mouse brachial LNs were inflamed using CFA (denoted as + CFA) or not (denoted as control). Then mice intraPAT injection of EαGFP (20 μg/ PAT) or FITC or TRITC painting on the skin. PAT and the adjacent LN were harvested 18 h later for imaging or flow cytometric analysis. A) Photomicrographs depicting distribution and density of EαGFP⁺ cells in PAT of control or CFA-treated mice. B) Total number of CD11c⁺EαGFP⁺YAc⁺ cells in PAT (upper panel) or LNs (lower panel) of control and CFA-treated mice. C) Images of PAT from mice painted with FITC or TRITC for 18 h. White arrows indicate the subcapsular sinus that feeds the conduit system in draining LNs. Scale bar, 50 μm. D) FITC (green) and TRITC (red) were painted together on mouse scapular back skin; 18 h later, the draining LN was collected for imaging analysis. Conduits (threadlike structures) in the LN are labeled with FITC but not TRITC. E) The total number of FITC⁺CD11c⁺ or TRITC⁺CD11c⁺ DCs in brachial LNs of control or CFA-treated mice. F) In control or CFA-treated mice, upper scapular skin was injected i.d. with EαGFP (40 μg/site) and the same skin site was painted with TRITC 9 h later. Draining LNs were collected 17 h after TRITC painting and the number of EαGFP⁺TRITC⁻CD11c⁺MHCII^{hi} (black bar), EαGFP⁺TRITC⁺CD11c⁺MHCII^{hi} (open bar), and EαGFP⁻TRITC⁺CD11c⁺MHCII^{hi} (gray bar) cells were quantified. Data depict mean ± SEM. *, P < 0.05; **, P < 0.01. All data were obtained from 3 independent experiments with more than 3 replicates per group in each experiment.